

# Minibasin depocentre migration during diachronous salt welding, offshore Angola

Zhiyuan Ge<sup>1</sup>  | Rob L. Gawthorpe<sup>1</sup>  | Atle Rotevatn<sup>1</sup>  | Leo Zijerveld<sup>1</sup> | Christopher A.-L. Jackson<sup>2</sup> | Ayodeji Oluboyo<sup>1,3,4</sup>

<sup>1</sup>Department of Earth Science, University of Bergen, Bergen, Norway

<sup>2</sup>Basins Research Group (BRG), Department of Earth Science & Engineering, Imperial College, London, UK

<sup>3</sup>School of Earth, Atmospheric and Environmental Sciences, University of Manchester, Manchester, UK

<sup>4</sup>PGS-Reservoir, Weybridge, UK

## Correspondence

Zhiyuan Ge, Department of Earth Science, University of Bergen, Bergen, Norway.  
Email: zhiyuan.ge@uib.no

## Funding information

University of Bergen

## Abstract

Salt tectonics is an important part of the geological evolution of many continental margins, yet the four-dimensional evolution of the minibasins, the fundamental building block of these and many other salt basins, remains poorly understood. Using high-quality 3D seismic data from the Lower Congo Basin, offshore Angola we document the long-term (>70 Myr) dynamics of minibasin subsidence. We show that, during the Albian, a broadly tabular layer of carbonate was deposited prior to substantial salt flow, diapirism, and minibasin formation. We identify four subsequent stages of salt-tectonics and related minibasin evolution: (i) thin-skinned extension (Cenomanian to Coniacian) driven by basinward tilting of the salt layer, resulting in the formation of low-displacement normal faults and related salt rollers. During this stage, local salt welding led to the along-strike migration of fault-bound depocentres; (ii) salt welding below the eastern part of the minibasin (Santonian to Paleocene), causing a westward shift in depocentre location; (iii) welding below the minibasin centre (Eocene to Oligocene), resulting in the formation of a turtle and an abrupt shift of depocentres towards the flanks of the bounding salt walls; and (iv) an eastward shift in depocentre location due to regional tilting, contraction, and diapir squeezing (Miocene to Holocene). Our study shows that salt welding and subsequent contraction are key controls on minibasin geometry, subsidence and stratigraphic patterns. In particular, we show how salt welding is a protracted process, spanning > 70 Myr of the salt-tectonic history of this, and likely other salt-rich basins. The progressive migration of minibasin depocentres, and the associated stratigraphic architecture, record weld dynamics. Our study has implications for the tectono-stratigraphic evolution of minibasins.

## KEYWORDS

depocentre migration, minibasin, offshore Angola, passive margin, salt tectonics, salt weld

# 1 | INTRODUCTION

A minibasin is a syn-kinematic succession of sediment that subsides into a body of salt (e.g. Jackson & Talbot, 1991; Peel, 2014a). Minibasins are commonly found in passive margin salt basins, such as the Gulf of Mexico (e.g. Hudec, Jackson, Vendeville, Schultz-Ela, & Dooley, 2011; Lamb, Toniolo, & Parker, 2006; Prather, Booth, Steffens, & Craig, 1998), the West African margin (e.g. Hudec & Jackson, 2004; Marton, Tari, & Lehmann, 2000) and the Brazil margin (e.g. Quirk et al., 2012), as well as cratonic salt basins such as the North and South Permian basins (e.g. Hodgson, Farnsworth, & Fraser, 1992), and the Precaspian Basin (e.g. Barde et al., 2002; Duffy et al., 2017; Jackson et al., 2019). Most studies have focused on the geometry and evolution of salt-related structures flanking the minibasins (e.g. diapirs) rather than the minibasins themselves. Because of this, certain dynamics of minibasin subsidence are not fully understood (e.g. Brun & Fort, 2011; Clark, Stewart, & Cartwright, 1998; Hudec & Jackson, 2007; Peel, 2014b; Rowan, Peel, & Vendeville, 2004; Rowan & Weimer, 1998; Trudgill, 2011; Vendeville & Jackson, 1992).

Current models for the initiation and subsidence of minibasins are based on the analysis of subsurface data (e.g. Hudec, Jackson, & Schultz-Ela, 2009; McBride, Rowan, & Weimer, 1998), as well as observations from numerical models (e.g. Goteti, Ings, & Beaumont, 2012; Peel, 2014a) and scaled physical experiments (e.g. Callot, Salel, Letouzey, Daniel, & Ringenbach, 2016; Fort, Brun, & Chauvel, 2004; Jackson & Vendeville, 1994; Warsitzka, Kley, & Kukowski, 2013). Essentially, a minibasin forms as a package of sediments sinks into underlying salt, which is consequently expelled into adjacent salt-cored highs. Subsidence may be driven by either sediment loading (i.e. excess density), extension or contraction (e.g. Hudec et al., 2009; Peel, 2014a). As a minibasin sinks into the underlying salt, the salt is gradually depleted, and ultimately, the minibasin comes into contact with the sub-salt strata, creating a salt weld (Jackson & Cramez, 1989; Jackson & Vendeville, 1994). After welding, salt mobilization is no longer a viable mechanism to accommodate further minibasin subsidence in the same location; subsidence can only then occur where salt is still available (Jackson & Hudec, 2017). However, such conceptual models for minibasin growth are oversimplified, ignoring the fact that, in many salt basins, the direction and amount of sediment supply, the location of minibasin initiation, and the primary salt thickness may all be highly variable. As a result, how and over what timescales minibasins subside and weld in 3D remains unclear. Moreover, as minibasin subsidence and subsequent salt welding have a direct impact on the formation of related salt structures, a better understanding of minibasin evolution and growth also improves our knowledge of the development of genetically related salt structures.

## Highlights

- We use high-quality seismic data to show depocentres record minibasin subsidence dynamics and associated salt weld processes
- Depocentres can migrate along- and across-strike under the control of salt weld.
- Salt weld can be a protracted, diachronous process spanning over tens of million years in a single minibasin.
- Salt-cored anticline can form by depocentre migration and associated salt welding.

The main goals of this analysis are to understand the relationship between minibasin development, and salt flow and welding, and how these processes interact in time and space. We have chosen a single minibasin that is very well-imaged in seismic reflection data from the Lower Congo Basin, offshore Angola. The high quality, well-calibrated 3D reflection seismic dataset allows us to conduct a detailed tectono-stratigraphic analysis of the three-dimensional growth of the selected minibasin (Figure 1).

# 2 | GEOLOGICAL SETTING

The Lower Congo Basin formed during the opening of the South Atlantic Ocean, following Early Cretaceous rifting and breakup of the Gondwana super-continent (e.g. Nürnberg & Müller, 1991). After rifting, an up to 1 km thick evaporite sequence was deposited in the late Aptian (Loeme Formation) during a marine transgression and a subsequent period of basin isolation and desiccation (Figure 2) (Anderson, Cartwright, Drysdall, & Vivian, 2000; Lavier, Steckler, & Brigaud, 2001). After salt deposition, a shallow marine clastic-carbonate succession (Pinda Group) was deposited in Albian; this unit records the beginning of open marine conditions along the margin (Anderson et al., 2000; Marton et al., 2000; Valle, Gjelberg, & Helland-Hansen, 2001).

From Albian times onward, margin tilting triggered salt mobilization and drove basin-wide salt tectonics, which is characterized by thin-skinned deformation of the cover strata overlying the Loeme salt (e.g. Marton et al., 2000; Valle et al., 2001). In detail, three structural domains are identified; updip and downdip domains of extension and contraction, respectively, separated by a domain of translation (e.g. Fort et al., 2004; Marton et al., 2000). From the Santonian until the Eocene, the claystone-dominated Iabe and Landana formations occurred as salt diapirs grew and minibasins subsided into the intraslope translational domain (Anderson et al., 2000; Marton et al., 2000; Valle et al., 2001) (Figure 2). The Oligocene Malembo Formation consists mainly

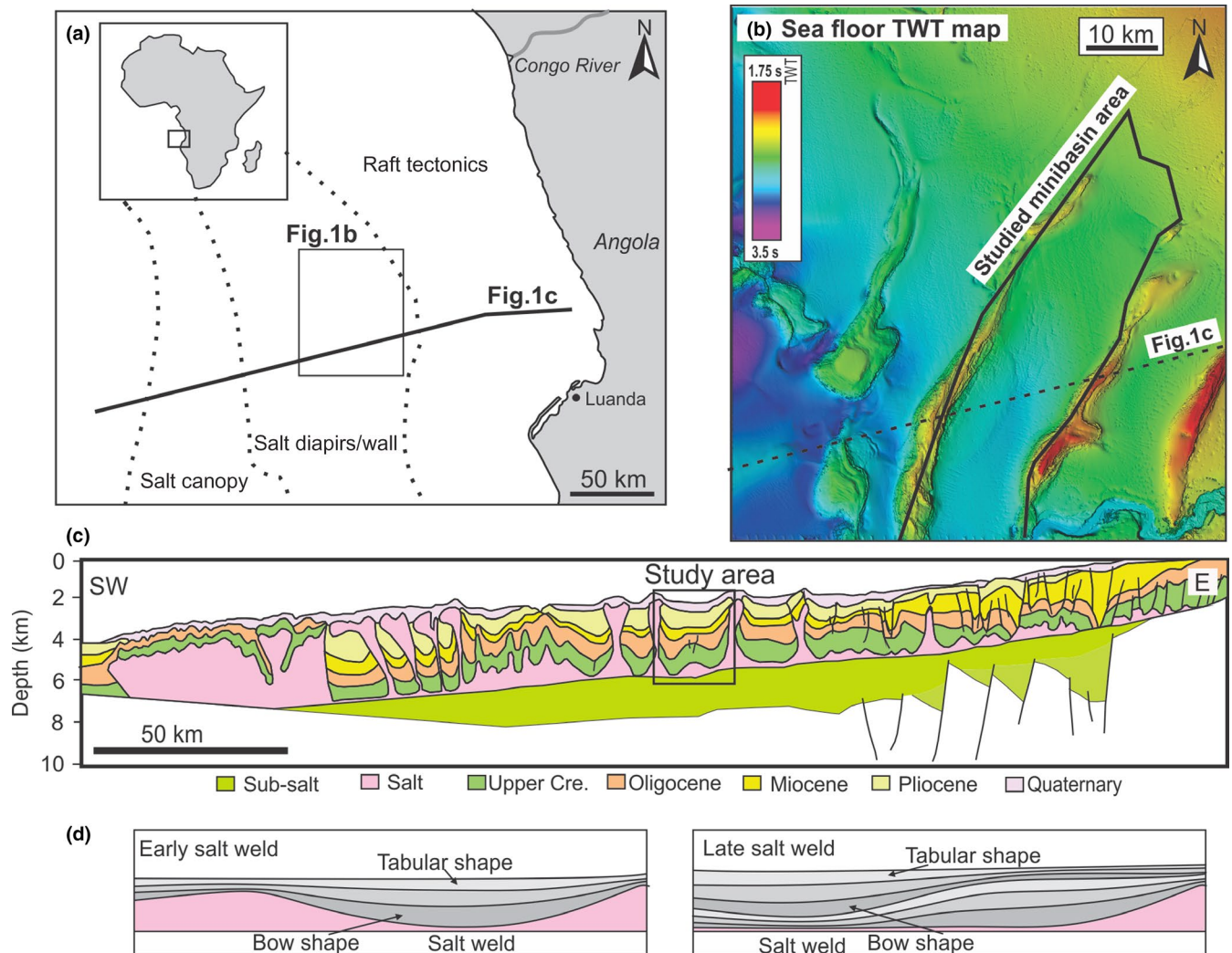


**FIGURE 1** (a) Simplified map showing the location and structural domains of the Lower Congo Basin (modified after Marton et al., 2000). The dotted lines are domain boundaries. Inset shows the geographical location of the Lower Congo Basin. (b) Seafloor TWT map of the intraslope area of the Lower Congo Basin. The salt walls and diapirs are visible as local bathymetric highs. The location is shown in (a). (c) Regional profile of the Lower Congo Basin (modified after Marton et al., 2000). Note the thin-skinned, upslope extension and downslope contraction system developed above the salt. Approximate location of the study area is indicated. The location of the profile is shown in (a) and (b). (d) Schematic diagram showing the stratal architecture during progressive salt welding (modified from Jackson & Hudec, 2017). Note the change of strata geometry from bow shape to tabular as salt welding occurs

of claystone interbedded with sandstone-rich turbidites (Anderson et al., 2000; Valle et al., 2001), with the increase in siliciclastic sediment being closely linked to the development of the Congo deepwater fan (Anka & Séranne, 2004). Miocene deepwater deposition of the Malembo Formation was increasingly confined by the bathymetric highs created by salt diapirs that were squeezed and inflating due to thin-skinned contraction triggered by regional uplift of the margin (Oluboyo, Gawthorpe, Bakke, & Hadler-Jacobsen, 2014). From the Pliocene onwards, silty and muddy sediments of the Malembo Formation were deposited in the Lower Congo Basin as the Congo fan delivered sediments to the northern part of the basin (Figure 2) (Anka & Séranne, 2004; Valle et al., 2001). Overall, the present-day margin tilt, as recorded

at the base of the salt layer, is ca.  $1.3^\circ$  (Marton et al., 2000; Peel, 2014b).

### 3 | DATA AND METHODS

#### 3.1 | Seismic and well data

This study utilises a high-quality, pre-stack time-migrated, three-dimensional seismic survey with a record length of six seconds two-way travel time (TWT), and inline and crossline spacing of 50 m. The seismic data are displayed with SEG normal polarity, where a downward increase in acoustic impedance is represented by a peak and is coloured in red in the displayed seismic profiles. The data quality is excellent in

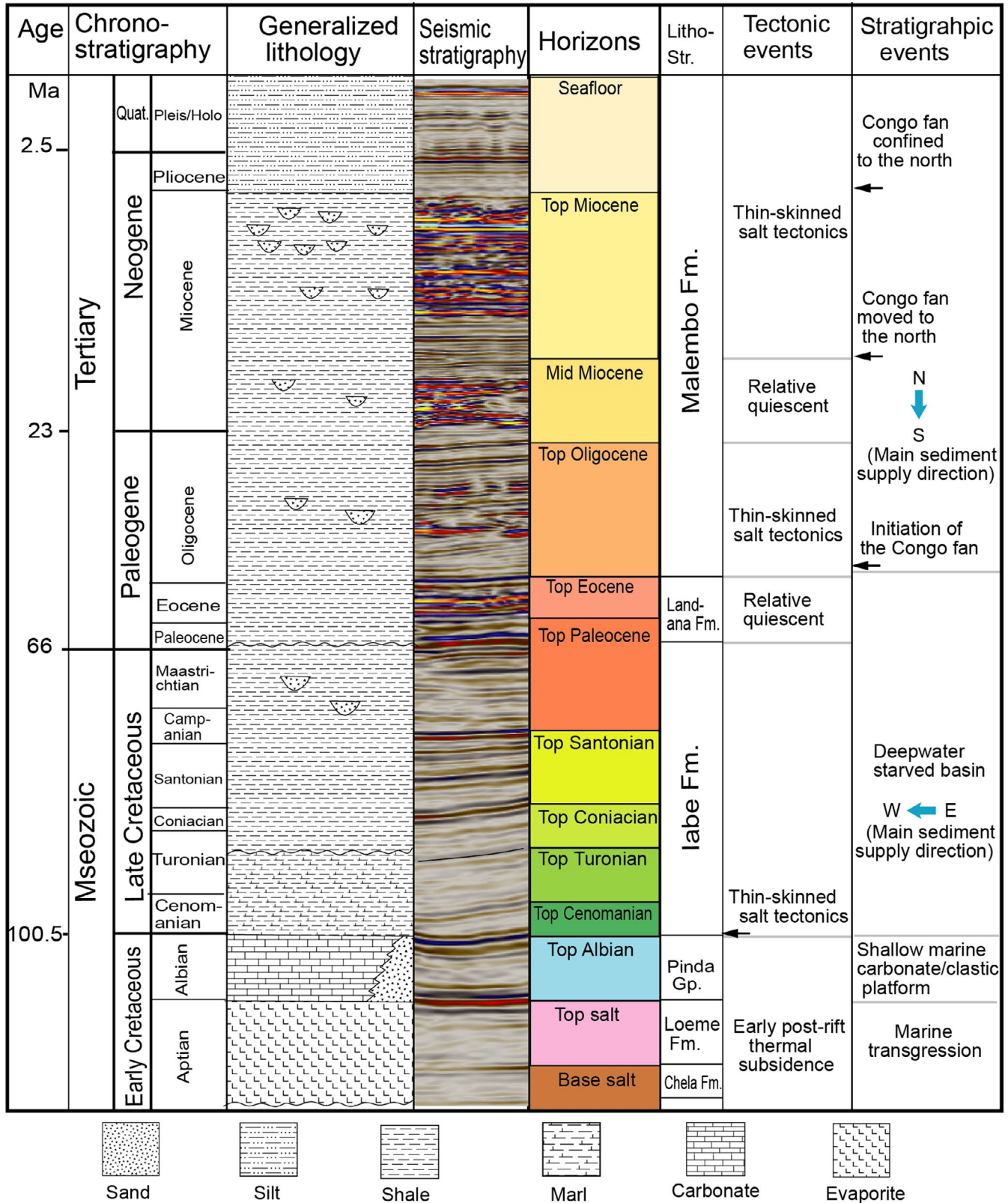


FIGURE 2 Stratigraphy of the Lower Congo Basin and interpreted horizons with major tectonic and stratigraphic events (modified after Anderson et al., 2000; Anka & Séranne, 2004; Valle et al., 2001)

the interval of interest, although it diminishes on the flanks of salt diapirs due to the presence of steeply dipping, up-turned minibasin strata. Assuming a seismic velocity range

of 2000–4000 m/s, and an overall downward decrease in peak frequency from 20 Hz to 40 Hz, we estimate the overall vertical seismic resolution ranges from 30 to 60 m (e.g.

Birch, 1960). Two proprietary wells located near to the seismic dataset contain conventional well-log data (e.g. gamma ray, sonic) that allow us to constrain minibasin lithology. Published age schemes provide some age constraints for our mapped seismic horizons (Anderson et al., 2000; Valle et al., 2001).

### 3.2 | Seismic interpretation

Thirteen horizons were mapped across the study area on the basis of stratal terminations and major changes in seismic facies (Figure 2). The horizons can be readily identified in the seismic dataset throughout the study area. The average interval between two horizons is 150–300 ms TWT up to the Eocene, which corresponds to 225–450 m (assuming an average seismic velocity of  $3,000 \text{ ms}^{-1}$ ). From the Paleocene onwards, seismic-stratigraphic packages are 400 to 800 ms TWT thick (600–1,200 m with assumed average seismic velocity of  $3,000 \text{ ms}^{-1}$ ). The base and top salt horizons delimit the Loeme salt, whereas the top salt and top Albian horizons bound a pre-kinematic succession deposited before the onset of major salt tectonics. The base salt horizon is affected by a strong velocity pull-up effect directly below salt structures, which are acoustically faster than surrounding, clastic-dominated minibasins (e.g. Figure 5a). The syn-kinematic interval, which records salt diapir growth and minibasin subsidence, extends from the top Albian to the seafloor (Figure 2). Following existing convention, all strata above top salt are referred as ‘cover’, and strata beneath base salt are referred to as ‘sub-salt strata’. The interpreted horizons allow sub-division of the cover into 11 stratal units (Figure 2).

### 3.3 | Time-thickness, cross-sections and salt weld

We calculated TWT thickness (isochron) maps of all 11 supra-salt stratigraphic units; thickness changes in these units, in conjunction with stratal geometries and seismic facies, are inferred to record spatial variations in salt-driven minibasin subsidence. One potential pitfall of this method relates to errors in the thickness calculations that could result from steeply dipping strata (typically on the flanks of salt diapirs bounding the minibasin) and lateral velocity variations (Marsh, Imber, Holdsworth, Brockbank, & Ringrose, 2010; Oluboyo et al., 2014). We have mitigated this effect by carefully cross-checking isochrons with the seismic sections to ensure thickness changes observed in one are observed in the other. As a result, our interpretation and analysis of isochrons are not affected by post-depositional, geometrical distortion. A second potential problem relates to uncertainties in defining the geometry of a depocentre, since the depocentre is represented simply by a relatively thick part of a specific stratigraphic interval. To better constrain depocentre

geometry, we define depocentres as the area corresponding to the upper 30% thick of the studied stratigraphic interval; contour lines with 50 or 100 ms TWT increment are used to illustrate depocentre location. Finally, since minibasins may translate during thin-skinned halokinesis (e.g. Dooley, Hudec, Pichel, & Jackson, 2018; Pichel, Peel, Jackson, & Huuse, 2018), the absolute locations of origin of the depocentres may be different from their present-day locations.

Previous studies have indicated that it is difficult to completely remove salt from a salt weld (Wagner, 2010; Wagner & Jackson, 2011) and, in practice, salt welds can contain tens of metres of remnant salt (Jackson, Rodriguez, Rotevatn, & Bell, 2014; Jackson, Zhang, Herron, & Fitch, 2018; Rowan, Lawton, & Giles, 2012; Wagner, 2010). Therefore, a seismically apparent weld may have up to 50 m of remnant salt (Wagner & Jackson, 2011). To quantitatively constrain the location of salt welds, we infer a weld where top and base salt horizons are less than 25 ms TWT apart, i.e. approximately 50 m assuming a seismic velocity of  $4,000 \text{ m/s}$  (e.g. Birch, 1960). Moreover, salt can weld on multiple stratigraphic levels (Wagner & Jackson, 2010). In this study, we mainly focus on primary salt welds in our welding process analysis (*sensu* Wagner & Jackson, 2010). A key assumption in our analysis is that the timing of salt welding can be estimated by variations in stratal geometries. More specifically, as a minibasin starts to weld, the geometry of stratigraphic interval changes from bowl- or wedge-shaped layers, to those with more limited thickness variations (e.g. tabular layers; Figure 1d) (Bouroulllec & Weimer, 2017; Jackson et al., 2019; Jackson & Hudec, 2017; Rowan & Weimer, 1998; Weimer et al., 2017).

## 4 | PRESENT DAY STRUCTURAL STYLE AND SALT DISTRIBUTION

The studied minibasin trends NNE, and is up to 16 km wide and 56 km long (Figures 1b and 3a). The minibasin is thickest in the southwest, with strata thinning and being upturned against flanking diapirs that are up to 2000 ms TWT tall (Figures 3b and 4).

Salt is generally very thin (<25 ms TWT) below the minibasin, suggesting a large part of the minibasin is welded (Figure 3c). Locally, however, three broadly NE-trending salt-related structures occur below the minibasin; these salt-related structures are up to 600 ms TWT thick, 6 km wide, and 17 km long (X–Z; Figure 3c and d). Among them are salt pillows X and Y, located in the NE and centre of the minibasin, respectively (Figures 3d, 4a, 5a and 6), and salt roller Z, which is bounded on its western side by a moderate throw (400 ms TWT), NW-dipping normal fault (Figures 3d and 5b). Two large salt walls bound the minibasin to the SE and NW; these are referred to as the SE and NW salt walls, respectively (Figure 3d).

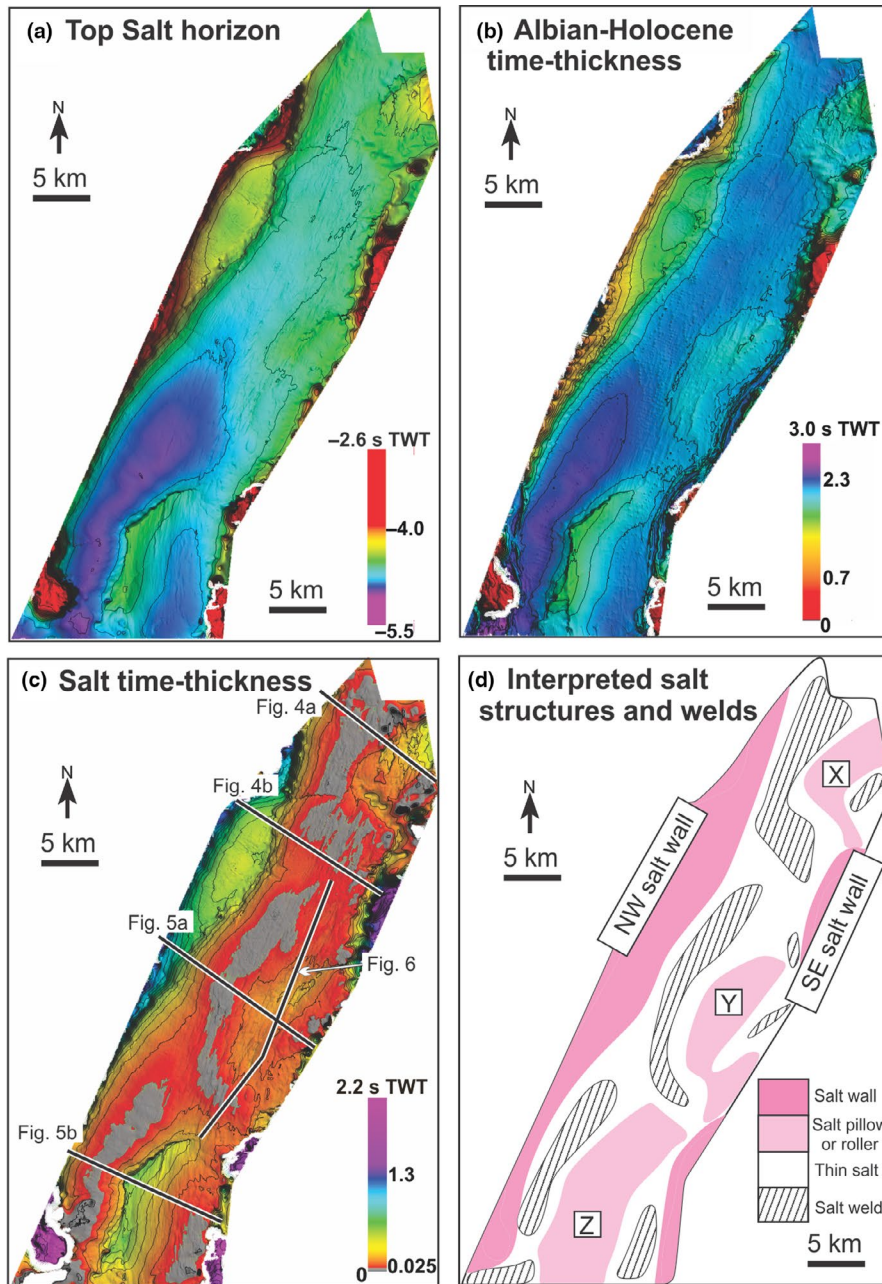


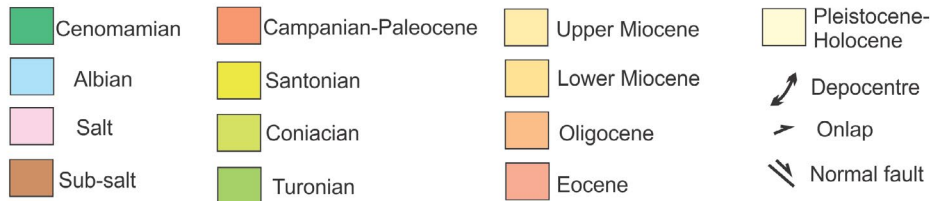
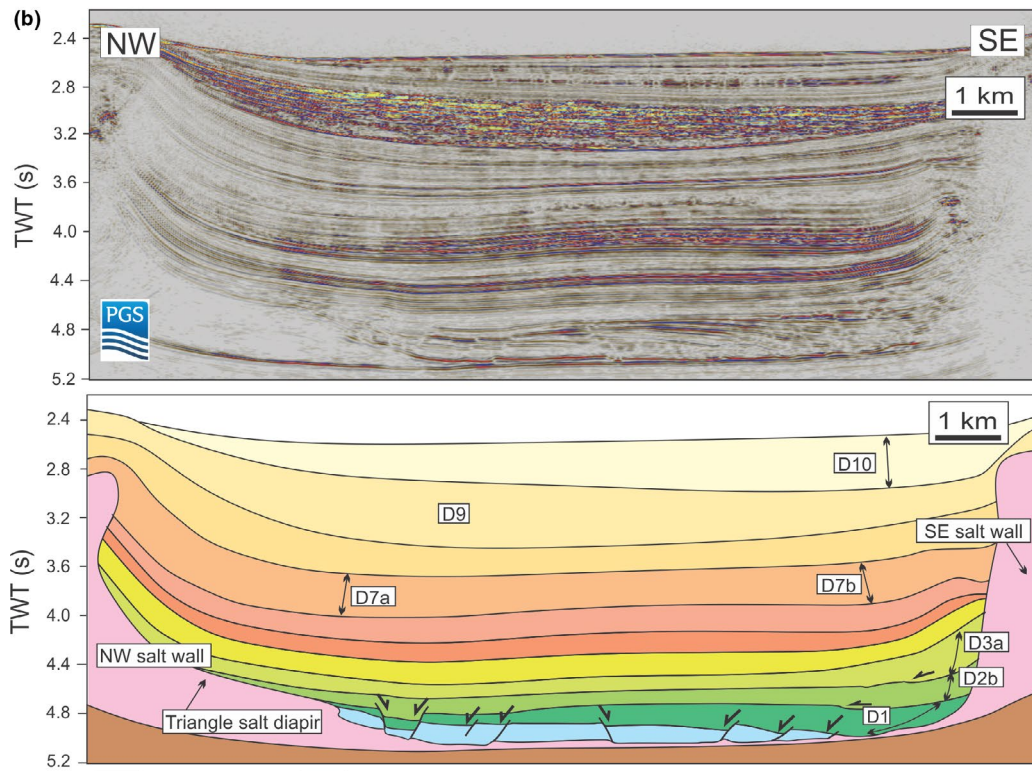
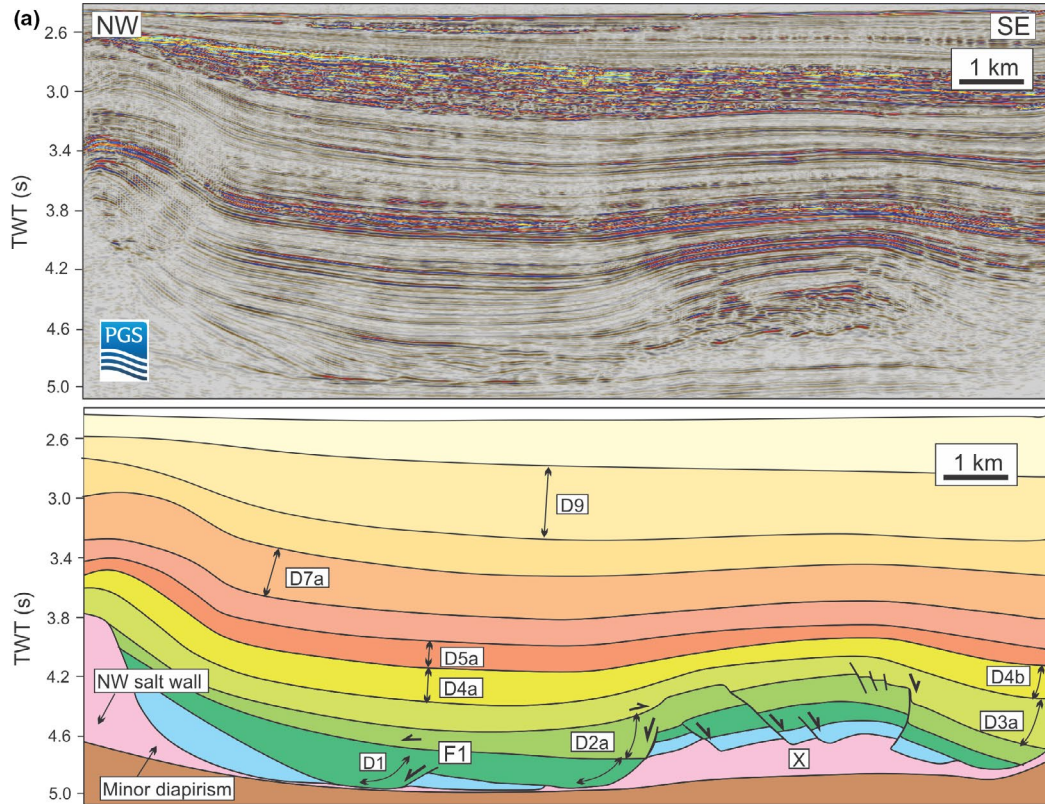
**FIGURE 3** TWT structure and time-thickness maps of the salt and supra-salt cover strata of the intraslope minibasin. (a) TWT structure map of the top salt horizon illustrating highs and lows of salt-related structures within the present-day minibasin. (b) Supra-salt cover time-thickness showing the thickness variations within the cover strata. Note that the thin supra-salt areas are thick salt areas in (c). (c) Salt time-thickness map, and its simplified sketch. (d) showing the location of salt welds (<25 ms TWT) and salt walls/diapir. Note the two salt pillows X, Y and one salt roller Z, located within the present-day minibasin

## 5 | SUPRA-SALT STRUCTURAL STYLE AND STRATIGRAPHIC ARCHITECTURE

Strata preserved within the minibasin shows significant temporal and spatial variations in geometry and thickness. The broadly tabular Albian succession, which sits directly on top

of the salt, is regarded as pre-kinematic (i.e. it was deposited prior to significant salt flow-induced deformation; Figure 7a). Based on stratal geometry and the relative locations of the depocentres, we divide subsequent minibasin development into four stages: (i) Cenomanian to Coniacian: depocentres initiation and lateral migration to the north and south (Figure 7b-d); (ii) Santonian to Paleocene: across-strike shift of minibasin depocentres to the west (Figure 7e and f); (iii) Eocene

**FIGURE 4** Seismic sections and interpretations of the northernmost part of the minibasin. (a) Seismic section (above) and interpretation (below) illustrate the structural style and stratigraphic architecture in the north of the minibasin. X is a salt pillow referred to in the text. D1 to D9 are depocentres referred to in the text. Note the growth strata of D1 and D2a along normal faults. For section location, see Figures 3c and 7a. (b) Seismic section (above) and interpretation (below) illustrating the structural style and stratigraphic architecture of the northern part of the minibasin, southwest of the section of Figure 4a. Note the growth strata of depocentres D1, D2b and D3a. D1, D2b, D3a, D7a, D7b, D9 and D10 are depocentres referred to in the main text. For section location, see Figures 3c and 7a



to Oligocene: turtle formation and abrupt shift of depocentres towards the flanks of the bounding salt walls (Figure 7g and h); and (iv) Miocene to present day: across-strike migration of depocentres (Figure 7i-k).

## 5.1 | Albian

### 5.1.1 | Description

The Albian succession is generally thin (average thickness of ca. 100 ms TWT) and broadly tabular (Figures 4 and 5), with only long length-scale changes in thickness being observed (Figure 7a). For example, the Albian thickens towards and is relatively thick (>300 ms TWT) in the NW of the study area (Figure 7a).

### 5.1.2 | Interpretation

The absence of major thickness variations suggests that the Albian was deposited during a period of overall tectonically quiescence, prior to salt-related deformation (Figure 7a). However, local thickness variations in the Albian indicate some salt flow and related diapirism may have occurred at this time, perhaps driven by sinking (downbuilding) of dense Albian carbonates into less dense, underlying Aptian salt (Figures 4a and 9a).

## 5.2 | Cenomanian to Coniacian

### 5.2.1 | Description

Small-scale normal faults, which are spaced 1–4 km and are 3–5 km long, and have up to 100 ms TWT of throw, offset the Albian to Coniacian succession (Figures 4 and 5). During the Cenomanian, the first major minibasin depocentre (D1) developed in the north of the study area (Figure 7b). The depocentre was ca. 27 km long and ca. 1.6 km wide (Figures 4 and 7b). In its northern part, the minibasins eastern boundary is defined by an abrupt thickness change of over 100 ms TWT, indicating a syn-depositional growth fault (F1; Figures 4a and 7b).

Two depocentres, which are offset from the Cenomanian depocentre (D1), characterise the Turonian interval (D2a and D2b; Figure 7c). The northern depocentre (D2a) is relatively small (c. 6 km long and ca. 6 km wide; Figure 7c) and offset

2 km east of the one defined in the underlying, Cenomanian succession (D1), lying immediately west of salt pillow X (Figures 4a and 8e). Depocentre D2b is ca. 27 km long and ca. 7 km wide, and is located against the SE salt wall in the central part of the minibasin (Figure 7c). A seismic profile shows the depocentre defines a south-eastwards-thickening wedge, expanding from < 100 ms TWT in the northwest to ca. 300 ms TWT in the southeast, documenting asymmetric subsidence linked to ongoing extension, and related salt flow and diapirism (Figure 5a). Specifically, thickening towards the southeast indicates the withdrawal of more salt from this location relative to the northwest (Figure 5a). Moreover, onlap of strata within depocentre D2b onto the top Cenomanian suggests the along strike migration of Depocentre D2b over Depocentre D1 (Figure 6).

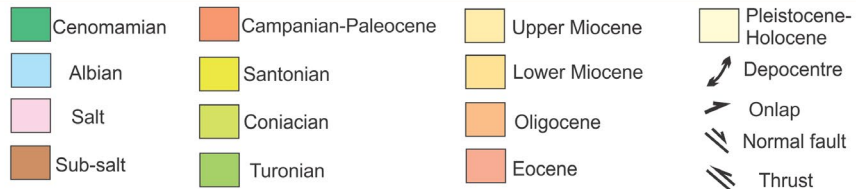
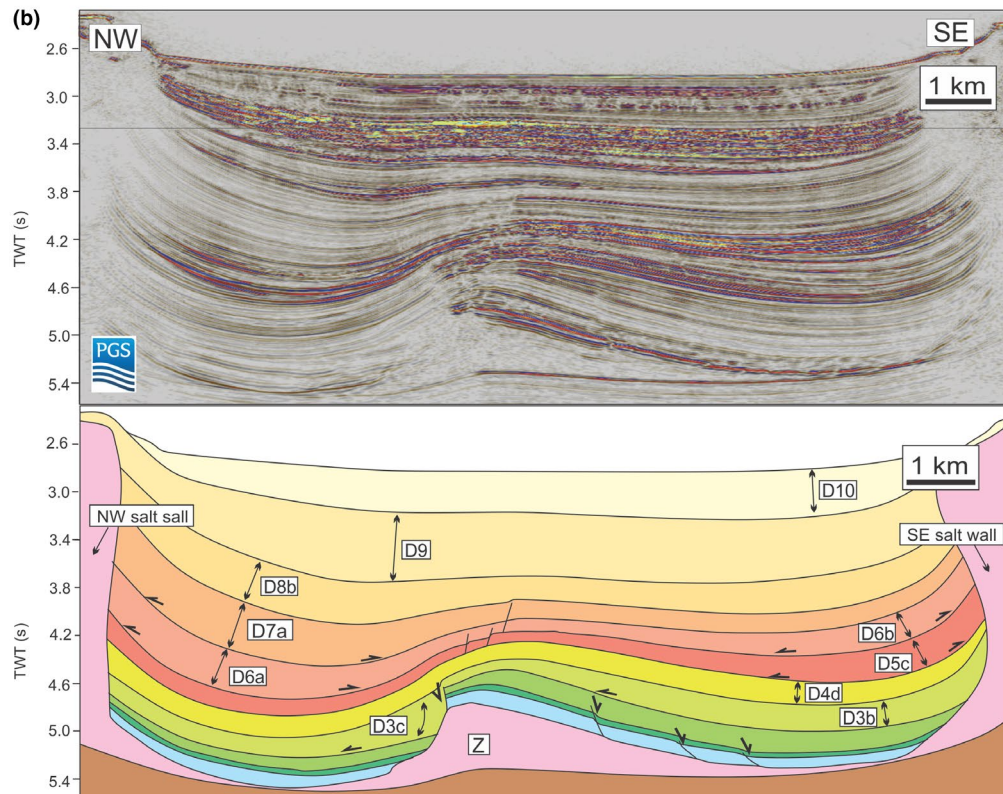
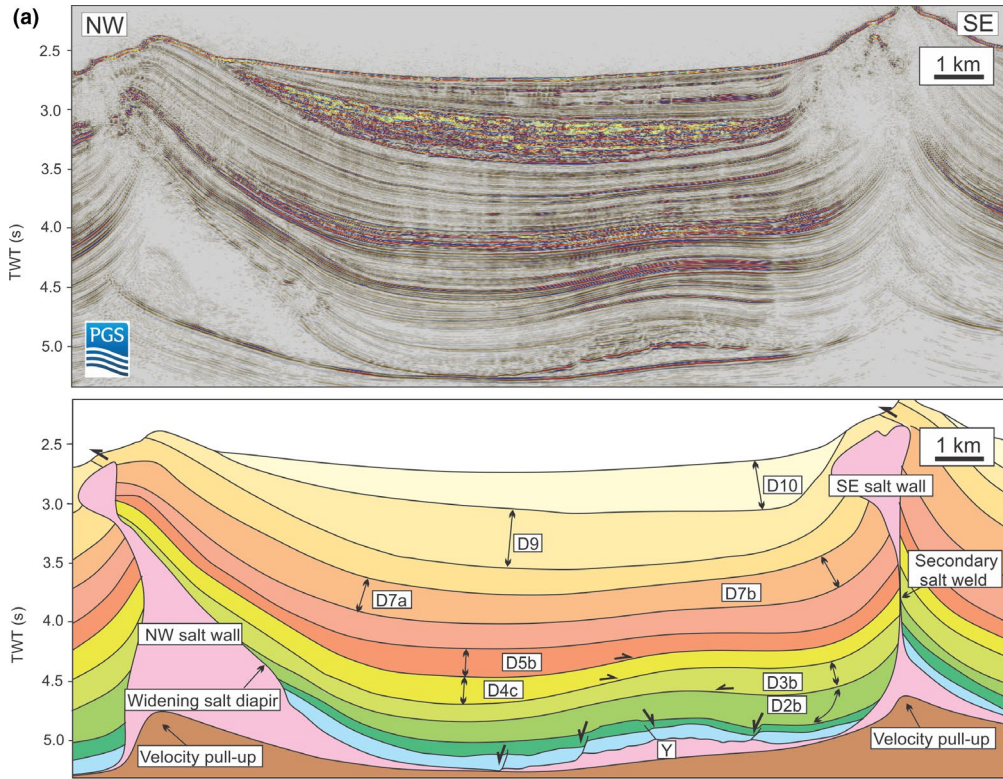
We distinguish three depocentres in the Coniacian interval; these are all offset to the southeastern side of the Turonian depocentres (Figure 7d). Depocentre D3a migrated to the east, relative to depocentres D1 and D2a, lying on the eastern side of salt pillow X (Figures 4a and 8e). Depocentre D3b is located against the SE salt wall, partly coinciding with the underlying depocentre (D2b) and bounding salt pillow Y in the east and south (Figures 5a, 6 and 7d). Depocentre D3c is approximately 1 km wide and 8–10 km long, and occurred along the western boundary of salt roller Z (Figure 5b). In cross section, depocentres D3b and D3c are both composed of growth wedges that thicken from < 100 ms TWT in the southwest to > 200 ms TWT in the east, suggesting asymmetrical subsidence and salt flow (Figure 5b). In other parts of the minibasin, normal faulting had largely ceased, with extension mainly accommodated by somewhat cryptic widening of salt diapirs (Figures 4b, 5a and 9d) (cryptic extension; *sensu* Jackson, Vendeville, & Schultz-Ela, 1994).

### 5.2.2 | Interpretation

Overall, the Cenomanian to Coniacian succession is characterized by the initiation and lateral migration of depocentres (Figure 8e). Depocentres developed during this stage are generally related to salt-detached extension and normal faulting. For example, depocentres D1–D3c thicken towards normal faults and extensional diapirs, which are thus inferred to be (re)actively growing at this time (Figures 4 and 5). Our local evidence for Cenomanian to Coniacian extension (Figure 9b–d) is consistent with regional evidence provided

**FIGURE 5** Seismic sections and interpretations of the central and southern part of the present-day minibasin. (a) Seismic section (above) and interpretation (below) illustrate the structural style and stratigraphic architecture in the central part of the minibasin. Y is a salt pillow referred in the text. D2a to D10 are depocentres referred to in the text. For section location, see Figures 3c and 7a. (b) Seismic section (above) and interpretation (below) illustrating the structural style and stratigraphic architecture of the southern part of the minibasin. D3b, D3c, D5c, D6a, D6b, D7a, D8b, D9 and D10 are depocentres referred in the main text. Note the normal fault-bounded depocentre D3c. Z is a salt roller referred to in the text. For section location, see Figure 3c or 7a





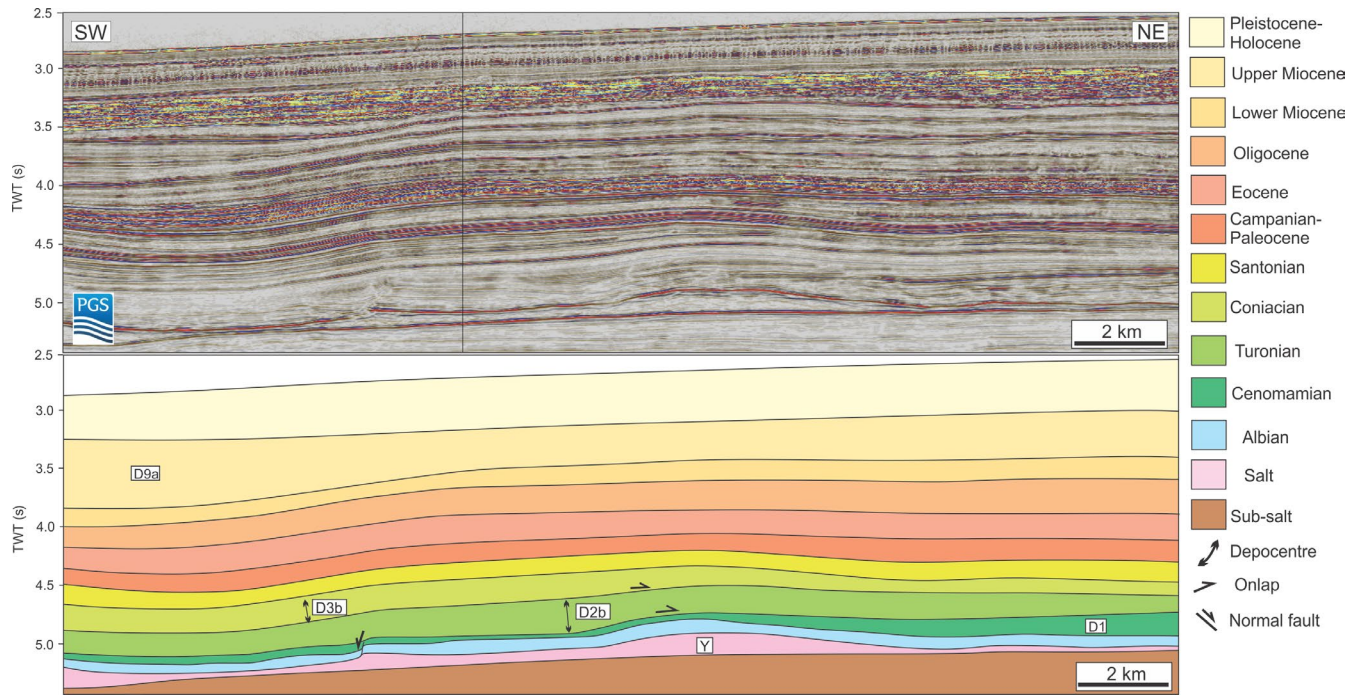


**FIGURE 6** Seismic section (above) and interpretation (below) illustrating the structural style and stratigraphic architecture along the strike of the minibasin. Note the onlap from D3a to D2b, and from D2b to D1, respectively. D1, D2b, D3a and D9 are depocentres referred in the text. Y is a salt pillow referred in the text. For section location, see Figure 3c or 7c

by Valle et al. (2001), who relate extension to thin-skinned gravity gliding of supra-salt cover driven by regional tilting.

Minibasin subsidence also initiated salt thinning and subsequent welding. For example, Depocentres D1 and D2b were superposed (Figure 4a) because there was sufficient salt beneath the northern corner of Depocentre D1 to allow continued subsidence. In contrast, by D2 times (i.e. Turonian), the southern part of Depocentre D1 had welded, with salt having flowed laterally into embryonic diapirs flanking the minibasin (Figure 9c and d). As a result, subsidence shifted along strike towards the south into a location where salt was still relatively thick and accommodation generation, driven by salt expulsion, was still ongoing (Figure 8e). This is evident by the Turonian strata laterally onlapping over the Cenomanian strata near Depocentre D1 (Figure 6). A similar process occurred in the Coniacian, when subsidence again shifted progressively along strike to the south (i.e. D3a and D3b are offset from depocentres D2a and D2b); we again infer this shift occurred in response to the onset of (local) welding (Figures 6, 7c and 8a). The minibasin was 500–700 ms TWT thick when welding is inferred to have occurred (e.g. Figure 5), which is in good agreement with an initial salt thickness of ca. 1 km (assuming a seismic velocity of  $4,000 \text{ ms}^{-1}$ ) (Lavietet al., 2001).

Progressive depocentre migration and related salt welding were also responsible for the formation of the salt pillows, with these remnant, albeit relatively thick salt bodies being

trapped below the subsiding minibasin (e.g. D2a and D3a bounding salt pillow X; Figure 4).

## 5.3 | Santonian to Paleocene

### 5.3.1 | Description

The Santonian times saw an abrupt westward shift in deposition (D4a and D4c; Figure 7e). In the northern part of the study area, two depocentres developed on the western and eastern side of salt pillow X (D4a and D4b; Figure 4a). Depocentre D4a strata are thick in the middle with  $> 260 \text{ ms TWT}$  and thin in its flanks of  $< 100 \text{ ms TWT}$  (Figure 4a). Depocentre D4b developed above, but is noticeably smaller than Depocentre D3a (Figure 4a). Further south, 260 ms TWT thick, Depocentre D4c developed in the western part of the minibasin, bounded by salt pillow Y and the NW salt wall (Figure 5a). Depocentre D4d, which is developed in the southeast, directly above Depocentre D3b, represents a minor exception to the broadly westward shift in subsidence (Figure 5b).

From the Campanian until the Paleocene, the subsidence regime was broadly similar to that characterising the Santonian (Figure 7f). Depocentres D5a, D5b and D5c formed above D4a, D4c and D4d, respectively (Figure 7d), with the main difference being that Depocentre D5a (3–4 km long and 1–2 km wide) was smaller than Depocentre D4a (Figure 8f), whereas depocentres D5b and D5c are considerably larger than their underlying depocentres (Figures 5b and 7f).

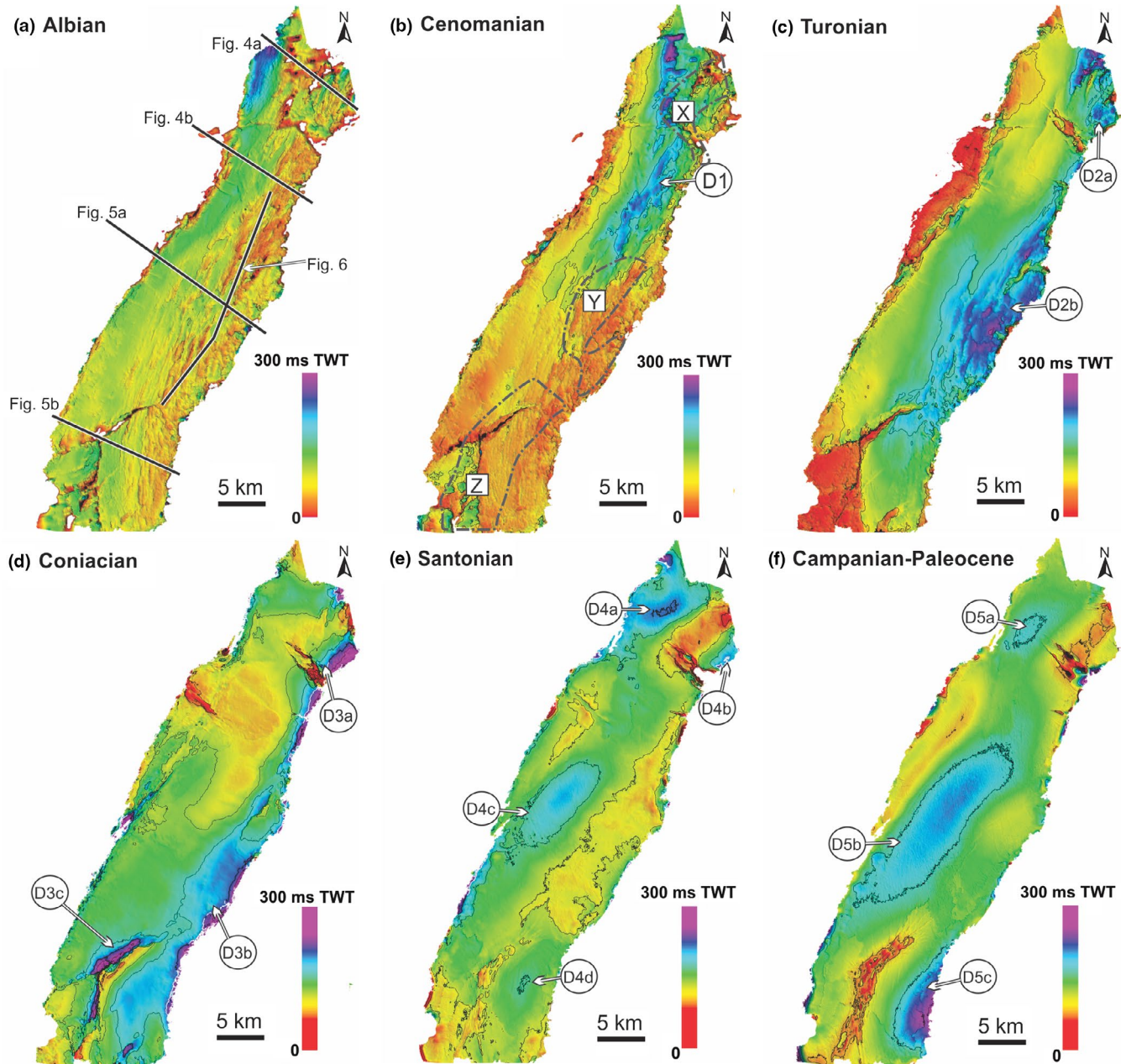


**FIGURE 7** Time-thickness maps for each of the nine supra-salt units considered in this study. The lines in 7a and g are seismic profile locations. The dash lines in 7b and h are present-day locations of salt-related structures X, Y and Z. (a) Albian: limited thickness variations, indicating a quiescent stage. (b) Cenomanian: widespread small normal faults and the development of Depocentre D1 controlled by normal faults. (c) Turonian: lateral migration of depocentres D2a and D2b. Note Depocentre D2b partially overlaps depocentre D1. (d) Coniacian: migration of depocentres D3a, D3b and D3c. (e) Santonian: development of new depocentres (D4a and D4c) to the west of the old depocentres (D3a and D3b), which remained active as D4b and D4d. (f) Campanian–Paleocene: growth of Depocentres D5a, D5b and D5c. (g) Eocene: development of Depocentres D6a and D6b along the flanks of the minibasin. (h) Oligocene: migration of Depocentres D7a and D7b in a northward direction. (i) Early Miocene: newly developed Depocentres D8a and D8a migrated to the west of the minibasin. (j) Later Miocene: elongate Depocentre D9 in the centre of the minibasin. (k) Pleistocene to Holocene: development of Depocentre D10 in the east of the minibasin

### 5.3.2 | Interpretation

In Santonian times, as large parts of minibasin below depocentres D3a and D3b welded (Figures 8b and 9d), subsidence shifted westwards (Figures 7e and 8f). Thinning of

strata towards the minibasin flanks, such as Depocentre D4a, indicates that the shift of minibasin downbuilding is due to excess density (cf. Hudec et al., 2009). At the same time, the presence of the two small depocentres D4b and D4d directly overlying D3a and D3b suggests that salt withdrawal

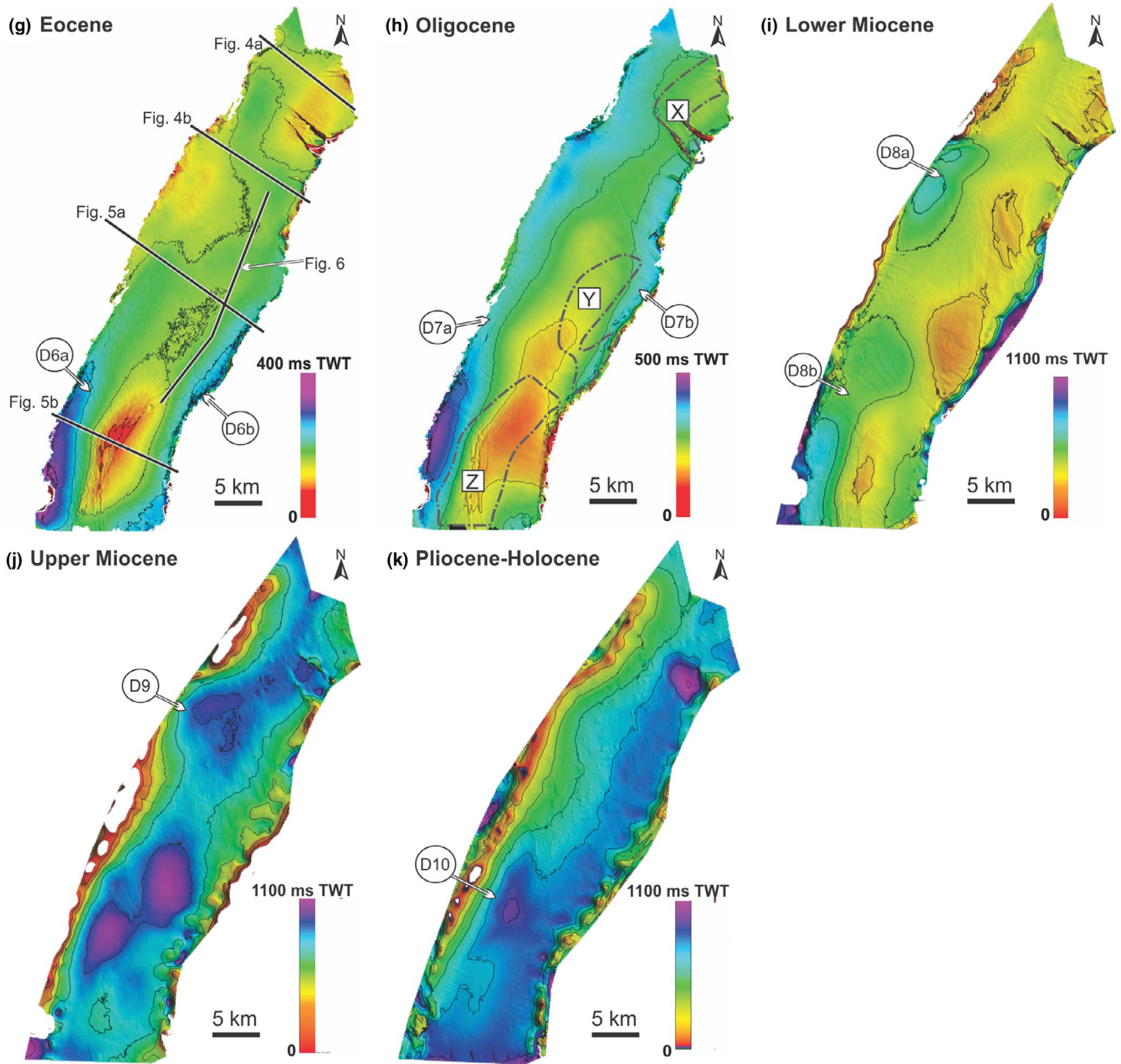


FIGURE 7 (Continued)

continued locally beneath existing depocentres (Figures 7e and 8f). Moreover, as observed in earlier time periods, salt pillows and walls continued to grow as salt became trapped between sub-basins within the subsiding minibasin (e.g. D4c and D5b, which separate salt pillow Y from the NW salt wall; Figures 5a and 8b).

## 5.4 | Eocene to Oligocene

### 5.4.1 | Description

During the Eocene and Oligocene, minibasin subsidence shifted to the immediate flanks of the adjacent

diapirs (Figures 5b and 7g). For example, during the Eocene, Depocentre D6a was located in the west of the minibasin, having shifted abruptly to this location from D5b (Figure 8f and g). Depocentre D6b progressively grew towards the east, extending over Depocentre D5c (Figures 7g and 8g). In cross section, depocentres D6a and D6b thicken outwards from ca. 80 ms TWT along the centre of the minibasin to > 350 ms TWT thick in the minibasin flanks (Figures 7g, 8f and g). Together, depocentres D6a and D6b define a turtle structure in the south of the minibasin (Figure 5b). The turtle grew and expanded north-eastwards during the Oligocene, as the two Eocene depocentres extended north-eastwards to form depocentres D7a and D7b (Figures 7h and 8g).

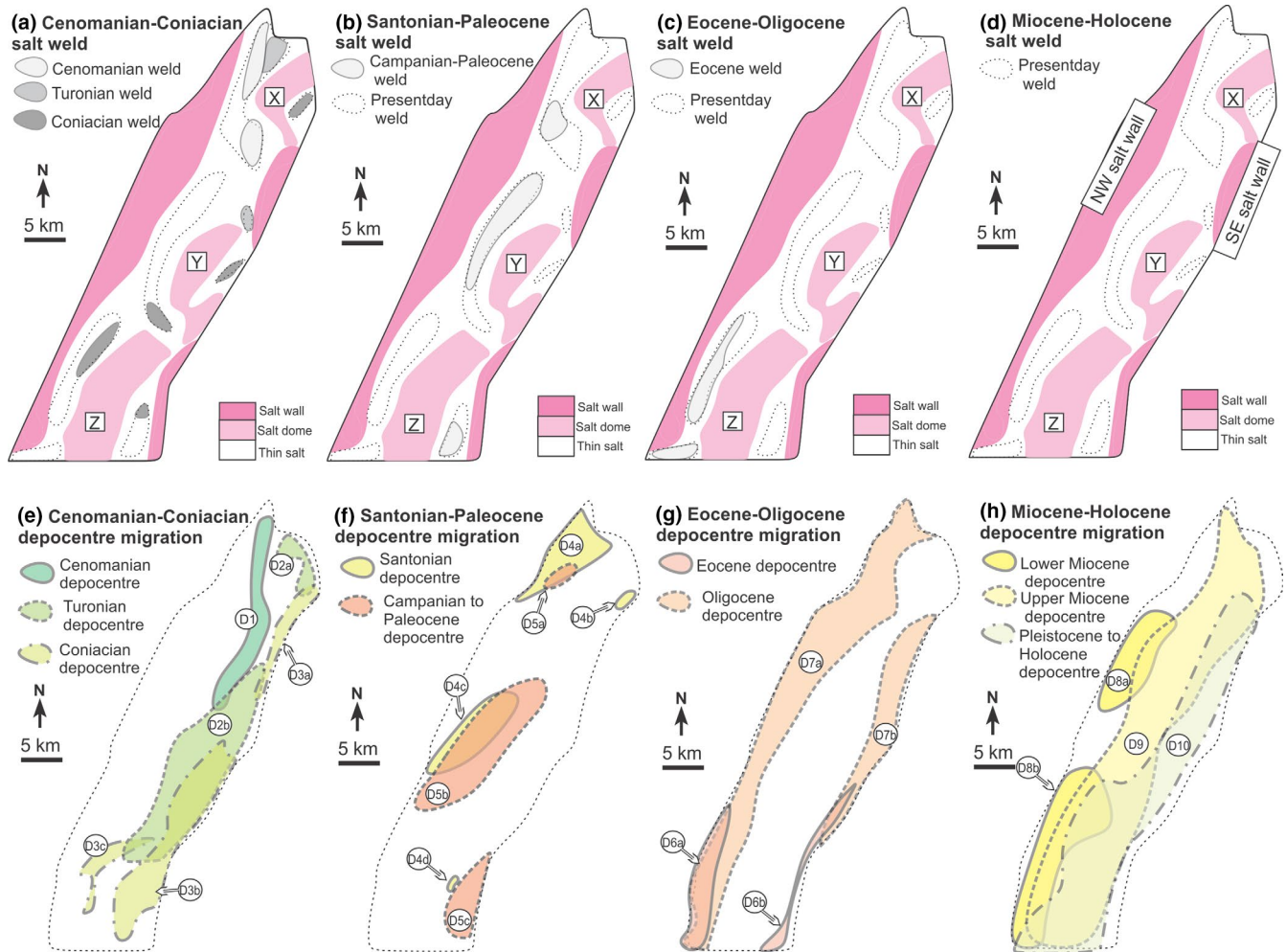


**FIGURE 8** Schematic diagram illustrating the four stages of depocentre migration and interpreted concurrent evolution of the salt weld in the minibasin. (a)–(d) Locations and sequences of salt weld: (a) Welding during depocentre lateral migration (Cenomanian to Coniacian); (b) Welding as depocentre migrating westwards across strike (Santonian to Paleocene); (c) Welding during turtle structure formation (Eocene to Oligocene); (d) No further salt weld (Miocene to Holocene). (e)–(h) Locations of depocentre occurrence and migration: (e) Initiation of first depocentre and subsequent lateral migration (Cenomanian to Coniacian); (f) Depocentres across-strike migration to the west (Santonian to Paleocene); (g) Migration of depocentres to the flanks of the minibasin and formation of turtle structure (Eocene to Oligocene); (h) Eastwards across-strike migration of depocentres (Miocene to Holocene)

## 5.4.2 | Interpretation

The Eocene and Oligocene represents a stage of turtle structure development (Figure 8g). In the Eocene, the turtle structure first appeared along salt roller Z in the southern part of the minibasin, later extending along strike to form a larger, basin-wide turtle structure in the Oligocene (Figure 7a and h). Although turtle structures may be driven by sediment loading and/or extension (Jackson et al., 1994), we interpret the main control in this case was for former due to the absence of extensional structures (e.g. normal faults) within age-equivalent strata (Figure 9i). Moreover, our interpretation is consistent with results arising from the regional study of Marton et al. (2000), who suggest the studied minibasin was in the intraslope translational domain despite contemporaneous

thin-skinned extension and contraction in the upslope and downslope area.

## 5.5 | Miocene to holocene

### 5.5.1 | Description

During the early Miocene, two depocentres developed above Depocentre D7a on the western side of the minibasin (D8a and D8b; Figures 5b and 7i). By the late Miocene, the minibasin is defined by a single, 4–9 km wide, NE-trending depocentre, the axis of which lies midway between the flanking salt walls (D9; Figure 7j). Overall, this succession thins towards flanking salt walls, suggesting that the latter were rising at this time (Figure 5). Subsequent subsidence

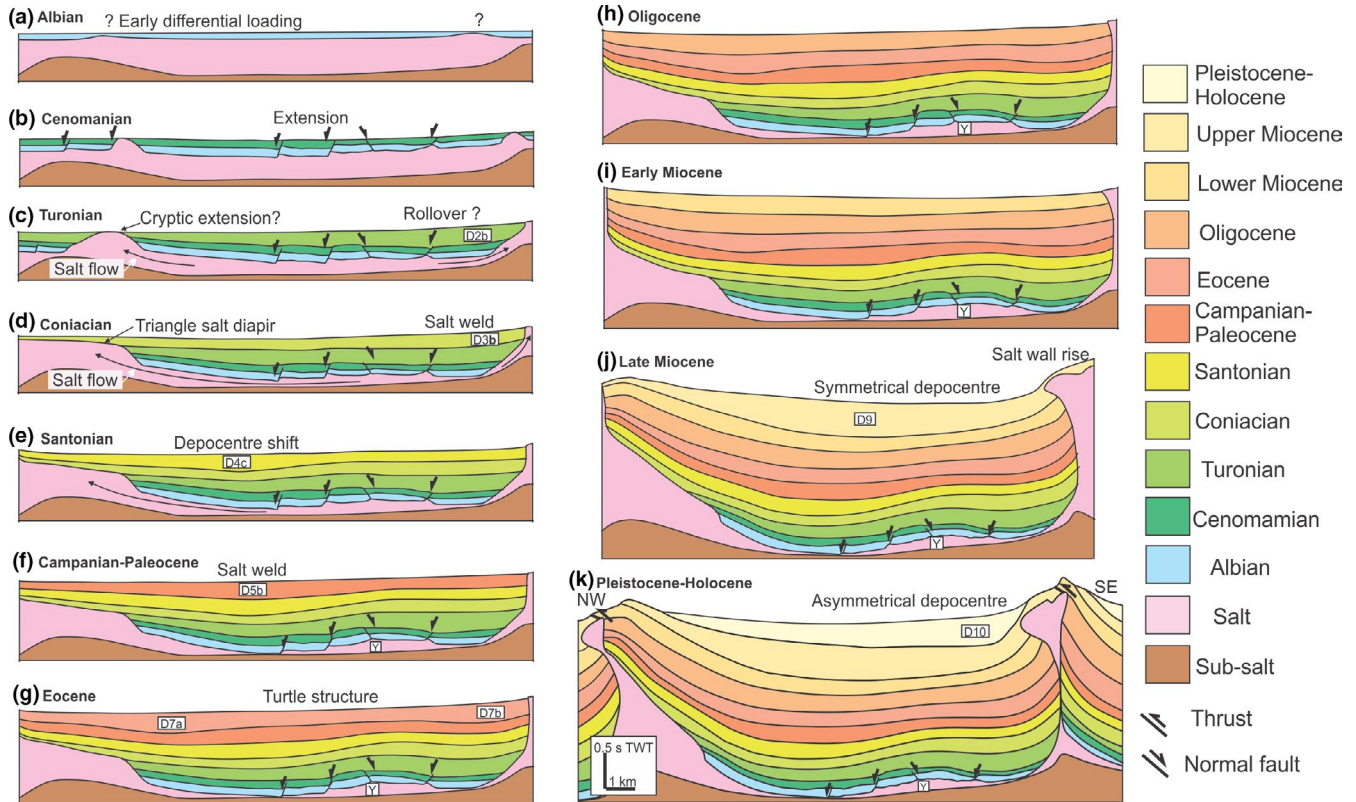


**FIGURE 9** Schematic diagram based on Figure 5a illustrating depocentre migration in the central part of the minibasin. (a) Albian: a relatively quiescent stage. (b)–(d) Cenomanian to Coniacian: depocentre migrated under extension, note the growth strata of Depocentre D2a and salt weld occurred before Depocentre D3a. (e)–(f) Santonian to Paleocene: deposition migrated across strike to the west of the minibasin. (g)–(h) Eocene: turtle structure developed as deposition focused on both sides of the minibasin. (i)–(k) Miocene to Holocene: depocentres migrated towards southeast due to elevated salt diapirs/walls. See text for discussion

occurred on a single 4–9 km wide, >600 ms TWT deep depocentre focused along the eastern side of the minibasin, ca. 5 km offset from the minibasin axis (D10; Figure 7k). Depocentre D10 is strongly asymmetrical, thinning towards northwest, as the northwest limb of the neighbouring minibasin is thrust over the southwest limb of the studied minibasin. A secondary salt weld (terminology after Wagner & Jackson, 2010) is locally developed between the two minibasins (Figure 5a).

### 5.5.2 | Interpretation

In Miocene times, subsidence migrated from the west of the minibasin towards the east, with this migration being more prominent in the northern than the southern part of the minibasin (Figure 8h). We infer this shift occurred due to margin tilting and regional contraction. In the early Miocene, margin tilting caused minibasin subsidence in the west so that sediment accumulated preferentially in this location (D8a and D8b; Figure 7i). In the late Miocene, contraction affected the intra-slope basin area, which is evident by the squeezed and uplifted salt walls. Further contraction in Pleistocene was accommodated by thrusting and secondary weld formation (Figures 5a and 9k).

## 6 | DISCUSSION

### 6.1 | Depocentre migration during minibasin development

Early studies of minibasin initiation and evolution have generally assumed that minibasin subsidence is driven by its excess density relative to underlying salt (e.g. Worrall & Snelson, 1989). Such mechanism is likely to be true during the later stages of minibasin development, when the sedimentary infill is both thick and dense, and thus negatively buoyant. However, it is very unlikely that this applies during the initial stage of subsidence, when the minibasin fill is thin and positively buoyant. Based on empirical density curves derived from well log data, Hudec et al. (2009) suggest a minibasin must be at least 2,300 m thick to sink under its own weight. Fernandez et al. (2017) recently suggest that the minibasin thickness required for density driven subsidence largely depends on the composition of the minibasin fill, as minibasins containing dense evaporite or carbonate may only need to be 1,000 m thick (or less) to subside. Instead of density-driven subsidence, a number of other processes can initiate minibasin formation when cover strata are still relatively

thin; these include, thin-skinned extension and contraction (e.g. Brun & Fort, 2011; Ings & Beaumont, 2010), differential loading (e.g. Ge, Jackson, & Vendeville, 1997; Peel, 2014a; Vendeville, 2005), and thick-skinned extension (e.g. Hudec et al., 2009; Jackson & Vendeville, 1994). However, it is problematic to apply these essentially two-dimensional models to the three-dimensional evolution of natural minibasins.

We document the full three-dimensional complexity of minibasin growth (and related welding; see below) over > 70 Myr. Major depocentre initiation was triggered by the onset of normal faulting in the Cenomanian, under the influence of regional extension and margin tilting (D1; Figure 4). Then, because the first generation of related depocentres (D1; Figure 4) welded, the next generation (Depocentre D2; Turonian) migrated to areas where salt was still thick and able to flow to create accommodation (Figures 6 and 9c). Since the flanking salt walls were relatively high due to the salt inflow, as indicated by the presence of upturned strata and thinning at the minibasin margins, the new depocentres were forced to migrate along strike (Figures 6 and 10). When the depocentres had welded along the eastern flank of the minibasin, the locus of deposition was forced to shift towards the northwest (Figures 5a, 8b and 9). However, as salt welding was a gradual process, some Santonian depocentres in the east (e.g. D4b and D4d; Figures 4a and 5b) directly overlay earlier-formed Coniacian depocentres (e.g. D3a and D3b; Figures 4b, 5 and 6). This process continued as the latest generation of depocentres welded (Figure 8c). Only when contraction commenced in the Miocene, did salt welding no

longer control depocentre migration (Figures 8d and 9i–k). The complex subsidence history recorded here contrasts with a minibasin growth model envisaging a single, bowl-shaped depocentre that sinks into salt and finally welds (e.g. Hudec et al., 2009; Jackson & Vendeville, 1994; Peel, 2014a; Vendeville & Jackson, 1992). For very large minibasins forming in a kinematically complex setting, where numerous salt bodies and minibasin controls interact, depocentres can progressively migrate or abruptly shift along and across strike, resulting in complex minibasin geometries and stratigraphic architectures (Figure 10). Therefore, the minibasin geometry might have an effect on the depocentre migration and welding evolution, with larger, more elongate minibasins more likely to have complex and protracted depocentre shifting and associated welding processes than the smaller, more ovate ones. As demonstrated by Fernandez, Hudec, Jackson, Dooley, and Duffy (2019), minibasins with relatively small size (c. 3 km wide) may only have one-time weld during their welding processes.

Previous studies demonstrate that shifts in depocentre position and minibasin tilting can be controlled by regional contraction (Hudec et al., 2009) or extension (Rowan & Weimer, 1998). Furthermore, it has also suggested that the shift of depocentre locations reflects minibasin welding (Figure 1d) (Jackson & Hudec, 2017; Rowan & Weimer, 1998). In the study area, shifts in depocentre position up until the Miocene were controlled by local salt welding, under the influence of extension (Figure 8a) and/or sedimentary loading (Figure 8b and c). Similar minibasin subsidence dynamics are observed

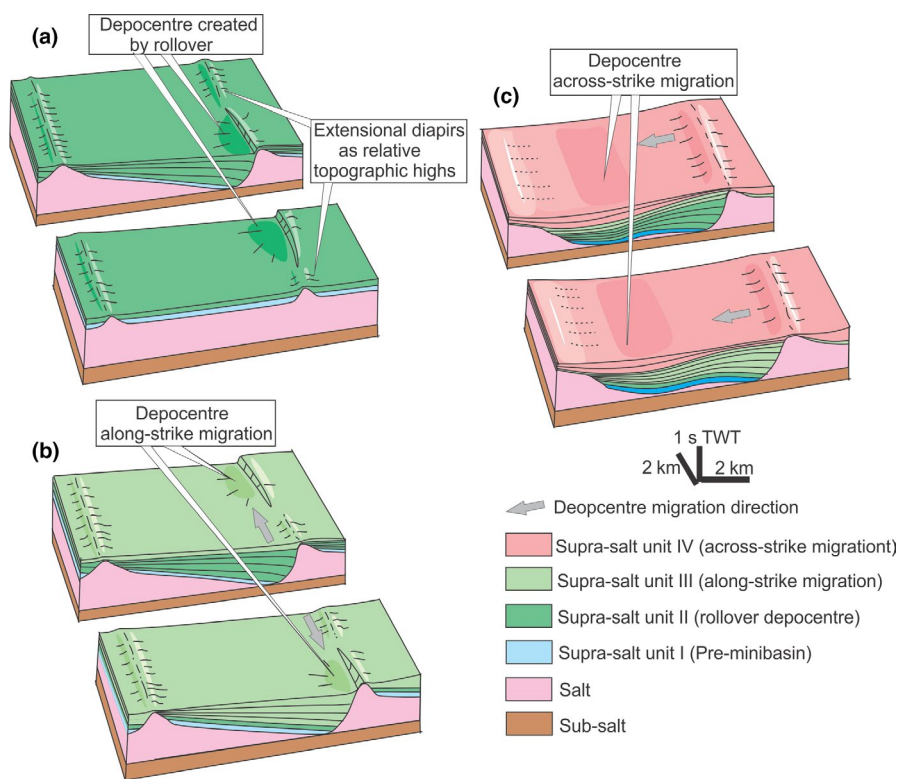


**FIGURE 10** Block diagram illustrating the along- and across-strike migration of depocentres and related salt weld within a single minibasin. (a) Minibasin/depocentre initiation by extension. Note the relative topographic highs of the extensional salt diapirs. (b) Depocentre along-strike migration due to salt weld and continued extension. (c) Depocentre across-strike migration due to salt weld beneath previous depocentres. Note the formation of the underlying salt pillow is different from the salt-cored anticlines associated with conventional turtle structures

in Permian minibasins of the Central North Sea (Stewart, 2007, their fig. 4; Stewart & Clark, 1999, their fig. 4b), where the shifts in depocentre location are observed during minibasin growth, driven by differential loading of denser anhydrite over less dense halite.

Another important question is why new depocentres form where they do and, therefore, why the pattern of depocentre migration is as it is? We suggest that the main control of the locations of new depocentres is salt availability with some secondary influences from seafloor topography (Figure 10). For example, Depocentres D3a, D2b and D3b were forced to migrate along strike due to the availability of thick salt along strike, as well as the slope gradient associated with flanking salt-wall highs (Figures 8e and 10b). Similar along-strike depocentre migration associated with thin-skinned extension is revealed by a field-based study in the Cotiella Basin, southern Pyrenees where depocentres shifted progressively along strike over 20 km with a time span of a few million years (López-Mir, Muñoz, & García-Senz, 2016; their fig. 9).

## 6.2 | Salt flow, trapping and welding

A number of studies have focused on salt flow in gravity-driven salt-tectonic systems, showing how salt flows in the dip direction (i.e. slope-parallel direction) (e.g. Brun & Fort, 2011; Cramez & Jackson, 2000; Duval, Cramez, & Jackson, 1992; Hudec & Jackson, 2004; Rowan et al., 2004). Even if it has long been known that salt flow and minibasin subsidence are three-dimensional (Rowan, 1993), it is difficult to constrain salt flow and related subsidence in the strike direction. In this study, we were not able to perform three-dimensional halokinetic-sequence analysis (Giles & Rowan, 2012) due to reduced seismic quality immediately adjacent to salt diapirs in areas of steeply dipping strata. As such, we could not precisely constrain how diapir rise and sediment accumulation rates, near the diapirs, varied both in time and space. However, the patterns of depocentre migration we identified suggest the flow of salt between different salt bodies was spatially and temporarily variable. For example, from the Cenomanian to Turonian, as the locus of deposition migrated southwards from D1 to D2b, the SE salt wall rose first in the northeast of the minibasin and then migrated towards the south (Figures 4b and 8a). The significant growth of NW salt wall formed even later, in the Santonian, after major depocentres shifted to the west of the minibasin (Figure 9e).

Our study also shows that a salt pillow or salt-cored anticline can simply be a piece of remnant salt trapped in the anticline due to progressive depocentre migration and accompanied three-dimensional salt flow. Such trapped salt need not result from turtle formation. Turtle structures form after minibasin welding, as both limbs of a minibasin subside and the intervening strata bend to form an anticline (Jackson et al., 1994). Salt-cored anticlines are thought only

occur beneath the turtle structure, as the minibasin flanks subside and weld quicker than the centre, trapping underlying salt (Jackson et al., 1994; Peel, 2014a). In the study area, salt pillow Y was not formed by a single stage of depocentre welding, nor by quicker subsidence of the minibasin flanks, but through progressive welding of multiple depocentres (Figure 3b). In essence, the northeastern, southern and western boundaries of salt pillow Y formed through salt welding in the Turonian, Cenomanian and Santonian to Paleocene, respectively (Figure 8). The conventional turtle structure only formed afterwards, during the Eocene and Oligocene, when the salt-cored anticline was already present, as two depocentres occurred on both sides of its flanks (Figure 9f and g).

A phenomenon that accompanies the migration of depocentres and progressive formation of salt pillows is the diachronous welding of salt, an observation made at the regional scale by studying multiple minibasins (Roberts, Metzgar, Liu, & Lim, 2004). Our study demonstrates that even within a single minibasin, the timing of salt welding is likely to be diachronous and spatially complex due to the ever-shifting locations of subsidence. Such process of protracted welding, over tens of million years, contrasts remarkably to the one-off salt welding of a minibasin suggested by current, largely two-dimensional models (e.g. Peel, 2014a; Vendeville & Jackson, 1992). Moreover, salt is generally assumed to be a good seal for hydrocarbons, especially those trapped in sub-salt strata (e.g. McBride et al., 1998; Rowan, 2004). However, welds, where salt is very thin to absent, can leak, allowing the migration of hydrocarbons from subsalt source rocks to supra-salt reservoirs. As such, identifying welds, and timing weld formation, are critical elements in the assessment of petroleum systems in salt basins. We show that salt welding can be spatially and temporarily very complex and hard to predict, meaning hydrocarbons may have to negotiate tortuous and ever-changing pathways between sources and reservoir rocks. Hydrocarbon exploration in minibasins therefore needs to consider the three-dimensional variations in salt welding.

## 7 | CONCLUSIONS

Our interpretation of high quality seismic reflection data from an intraslope minibasin in the Lower Congo Basin permits a detailed analysis of structural and stratigraphic evolution of the minibasin development and related salt flow. Interpreting closely-spaced horizons allows us to develop a high resolution tectono-stratigraphic framework that reveals, in some detail, a history of depocentre and subsidence migration, salt trapping and salt welding.

The time-thickness maps show the minibasin in this study is the result of amalgamation of multiple depocentres.



Following an Albian pre-kinematic stage, we identify four stages of depocentre migration: 1. Depocentre initiation and lateral migration under extension from Cenomanian to Coniacian; 2. Across-strike shift of depocentres to the west under the control of sedimentary loading from Santonian to Paleocene; 3. Turtle structure formation under sedimentary loading from Eocene to Oligocene; 4. Across-strike migration of depocentres under regional tilting and contraction.

Our analysis of the minibasin has allowed us to identify the driving forces for minibasin growth and the controls of depocentre migration in space and time. The early initiation and lateral migration of depocentres within the minibasin are largely controlled by thin-skinned extension. However, the exact timing of depocentre shift is closely linked to salt flow and welding. As early depocentres weld on sub-salt strata, later depocentres are forced to migrate to places where salt withdraw is still ongoing. In contrast, after the minibasin has largely welded, later contraction squeezes the salt walls and creates salt highs, forcing the depocentres to migrate to topographic lows within the minibasin. Moreover, the shift of depocentre location and subsequently salt welding also result in complex salt flow which, in turn, plays a significant role in formation of salt-related structures. Trapping of remnant salt by diachronous salt welding can form salt pillows underneath minibasins over protracted periods of time, spanning of more than 70 Myr.

This study demonstrates that the minibasin infilling geometry is the result of three-dimensional depocentre migration and salt flow, which may also be present during minibasin growth in other salt basins. Moreover, the protracted and complex welding processes during minibasin growth also have important implications for salt-related structures formation and hydrocarbon migration. Consequently, current models of minibasin growth need to take into account the spatial and temporal variations of minibasin evolution and welding processes, when interpreting the minibasin geometries and linking them to salt tectonic processes.

## ACKNOWLEDGEMENTS

This study was supported by Equinor AS under Turbidites, Topography and Tectonics (T<sup>3</sup>) project. We thank Sonangol, PGS and Equinor for providing access to well and seismic data from the Lower Congo Basin. Schlumberger is thanked for providing the Petrel software in the 3D Seismic Lab at the University of Bergen. We thank Naiara Fernandez and Jaume Vergés for reviews that improved the manuscript. We also thank the editor, Cynthia Ebinger, for editing the paper.

## CONFLICT OF INTEREST

There are no conflict of interest.

## DATA AVAILABILITY STATEMENT

The data that support the findings of this study are available from PGS. Restrictions apply to the availability of these data, which were used under license for this study.

## ORCID

Zhiyuan Ge  <https://orcid.org/0000-0002-6029-5512>

Rob L. Gawthorpe  <https://orcid.org/0000-0002-4352-6366>

Atle Rotevatn  <https://orcid.org/0000-0002-8413-3294>

## REFERENCES

- Anderson, J. E., Cartwright, J., Drysdall, S. J., & Vivian, N. (2000). Controls on turbidite sand deposition during gravity-driven extension of a passive margin: Examples from Miocene sediments in Block 4, Angola. *Marine and Petroleum Geology*, 17(10), 1165–1203. [https://doi.org/10.1016/S0264-8172\(00\)00059-3](https://doi.org/10.1016/S0264-8172(00)00059-3)
- Anka, Z., & Séranne, M. (2004). Reconnaissance study of the ancient Zaire (Congo) deep-sea fan. (ZaiAngo Project). *Marine Geology*, 209(1), 223–244. <https://doi.org/10.1016/j.margeo.2004.06.007>
- Barde, J.-P., Chamberlain, P., Galavazi, M., Harwijanto, J., Marsky, J., Gralla, P., & van den Belt, F. (2002). Sedimentation during halokinesis: Permo-Triassic reservoirs of the Saigak field, Precaspian basin. *Kazakhstan. Petroleum Geoscience*, 8(2), 177–187. <https://doi.org/10.1144/petgeo.8.2.177>
- Birch, F. (1960). The velocity of compressional waves in rocks to 10 kilobars: 1. *Journal of Geophysical Research*, 65(4), 1083–1102. <https://doi.org/10.1029/JZ065i004p01083>
- Bouroullec, R., & Weimer, P. (2017). Geometry and kinematics of Neogene allochthonous salt systems in the Mississippi Canyon, Atwater Valley, western Lloyd Ridge, and western DeSoto Canyon protraction areas, northern deep-water Gulf of Mexico. *AAPG Bulletin*, 101(7), 1003–1034. <https://doi.org/10.1306/09011609186>
- Brun, J.-P., & Fort, X. (2011). Salt tectonics at passive margins: Geology versus models. *Marine and Petroleum Geology*, 28(6), 1123–1145. <https://doi.org/10.1016/j.marpetgeo.2011.03.004>
- Callot, J.-P., Salel, J.-F., Letouzey, J., Daniel, J.-M., & Ringenbach, J.-C. (2016). Three-dimensional evolution of salt-controlled minibasins: Interactions, folding, and megaflap development. *AAPG Bulletin*, 100(9), 1419–1442. <https://doi.org/10.1306/03101614087>
- Clark, J., Stewart, S., & Cartwright, J. (1998). Evolution of the NW margin of the North Permian Basin, UK North Sea. *Journal of the Geological Society, London*, 155(4), 663–676. <https://doi.org/10.1144/gsjgs.155.4.0663>
- Cramez, C., & Jackson, M. P. A. (2000). Superposed deformation straddling the continental-oceanic transition in deep-water Angola. *Marine and Petroleum Geology*, 17(10), 1095–1109. [https://doi.org/10.1016/S0264-8172\(00\)00053-2](https://doi.org/10.1016/S0264-8172(00)00053-2)
- Dooley, T. P., Hudec, M. R., Pichel, L. M., & Jackson, M. P. A. (2018). *The impact of base-salt relief on salt flow and suprasalt deformation patterns at the autochthonous, paraautochthonous and allochthonous level: Insights from physical models* (p. 476). London, Special Publications: Geological Society.

- Duffy, O. B., Fernandez, N., Hudec, M. R., Jackson, M. P., Burg, G., Dooley, T. P., & Jackson, C.-A.-L. (2017). Lateral mobility of minibasins during shortening: Insights from the SE Precaspian Basin, Kazakhstan. *Journal of Structural Geology*, *97*, 257–276. <https://doi.org/10.1016/j.jsg.2017.02.002>
- Duval, B., Cramez, C., & Jackson, M. P. A. (1992). Raft tectonics in the Kwanza basin, Angola. *Marine and Petroleum Geology*, *9*(4), 389–404. [https://doi.org/10.1016/0264-8172\(92\)90050-O](https://doi.org/10.1016/0264-8172(92)90050-O)
- Fernandez, N., Duffy, O. B., Hudec, M. R., Jackson, M. P. A., Burg, G., Jackson, C. A. L., & Dooley, T. P. (2017). The origin of salt-encased sediment packages: Observations from the SE Precaspian Basin (Kazakhstan). *Journal of Structural Geology*, *97*, 237–256. <https://doi.org/10.1016/j.jsg.2017.01.008>
- Fernandez, N., Hudec, M. R., Jackson, C. A., Dooley, T. P., & Duffy, O. B. (2019). The competition for salt and kinematic interactions between minibasins during density-driven subsidence: observations from numerical models. <https://doi.org/10.31223/osf.io/jak5u>
- Fort, X., Brun, J.-P., & Chauvel, F. (2004). Salt tectonics on the Angolan margin, synsedimentary deformation processes. *AAPG Bulletin*, *88*(11), 1523–1544. <https://doi.org/10.1306/06010403012>
- Ge, H., Jackson, M. P., & Vendeville, B. C. (1997). Kinematics and dynamics of salt tectonics driven by progradation. *AAPG Bulletin*, *81*(3), 398–423.
- Giles, K. A., & Rowan, M. G. (2012). Concepts in halokinetic-sequence deformation and stratigraphy. *Geological Society, London, Special Publications*, *363*(1), 7–31. <https://doi.org/10.1144/SP363.2>
- Goteti, R., Ings, S. J., & Beaumont, C. (2012). Development of salt minibasins initiated by sedimentary topographic relief. *Earth and Planetary Science Letters*, *339–340*, 103–116. <https://doi.org/10.1016/j.epsl.2012.04.045>
- Hodgson, N. A., Farnsworth, J., & Fraser, A. J. (1992). Salt-related tectonics, sedimentation and hydrocarbon plays in the Central Graben, North Sea, UKCS. *Geological Society, London, Special Publications*, *67*(1), 31–63. <https://doi.org/10.1144/GSL.SP.1992.067.01.03>
- Hudec, M. R., & Jackson, M. P. A. (2004). Regional restoration across the Kwanza Basin, Angola: Salt tectonics triggered by repeated uplift of a metastable passive margin. *AAPG Bulletin*, *88*(7), 971–990. <https://doi.org/10.1306/02050403061>
- Hudec, M. R., & Jackson, M. P. A. (2007). Terra infirma: Understanding salt tectonics. *Earth-Science Reviews*, *82*(1), 1–28.
- Hudec, M. R., Jackson, M. P. A., & Schultz-Ela, D. D. (2009). The paradox of minibasin subsidence into salt: Clues to the evolution of crustal basins. *Geological Society of America Bulletin*, *121*(1–2), 201–221.
- Hudec, M. R., Jackson, M. P. A., Vendeville, B. C., Schultz-Ela, D. D., & Dooley, T. P. (2011). The salt mine: A digital atlas of salt tectonics.
- Ings, S. J., & Beaumont, C. (2010). Shortening viscous pressure ridges, a solution to the enigma of initiating salt ‘withdrawal’ minibasins. *Geology*, *38*(4), 339–342.
- Jackson, C.-A.-L., Duffy, O. B., Fernandez, N., Dooley, T. P., Hudec, M. R., Jackson, M. P. A., & Burg, G. (2019). The stratigraphic record of Minibasin subsidence, Precaspian basin, Kazakhstan. *Basin Research*, 1–25. <https://doi.org/10.1111/bre.12393>
- Jackson, C.-A.-L., Rodriguez, C. R., Rotevatn, A., & Bell, R. E. (2014). Geological and geophysical expression of a primary salt weld: An example from the Santos Basin. *Brazil. Interpretation*, *2*(4), SM77–SM89.
- Jackson, C.-A.-L., Zhang, Y., Herron, D. A., & Fitch, P. J. R. (2018). Subsurface expression of a salt weld. *Gulf of Mexico. Petroleum Geoscience*, *25*(1), 102–111.
- Jackson, M. P. A., & Cramez, C. (1989). Seismic recognition of salt welds in salt tectonics regimes. Paper presented at the Gulf of Mexico salt tectonics, associated processes and exploration potential: Gulf Coast Section SEPM Foundation 10th Annual Research Conference.
- Jackson, M. P. A., & Hudec, M. R. (2017). *Salt tectonics: Principles and practice*. Cambridge, UK: Cambridge University Press.
- Jackson, M. P. A., & Talbot, C. J. (1991). *A glossary of salt tectonics: Bureau of Economic Geology*. Austin, TX: University of Texas at Austin.
- Jackson, M. & Vendeville, B. C. (1994). Regional extension as a geologic trigger for diapirism. *Geological Society of America Bulletin*, *106*(1), 57–73. [https://doi.org/10.1130/0016-7606\(1994\)106<0057:REAAGT>2.3.CO;2](https://doi.org/10.1130/0016-7606(1994)106<0057:REAAGT>2.3.CO;2)
- Jackson, M. P. A., Vendeville, B. C., & Schultz-Ela, D. D. (1994). Structural dynamics of salt systems. *Annual Review of Earth and Planetary Sciences*, *22*, 93–117. <https://doi.org/10.1146/annurev.ev.22.050194.000521>
- Lamb, M. P., Toniolo, H., & Parker, G. (2006). Trapping of sustained turbidity currents by intraslope minibasins. *Sedimentology*, *53*(1), 147–160. <https://doi.org/10.1111/j.1365-3091.2005.00754.x>
- Lavier, L. L., Steckler, M. S., & Brigaud, F. (2001). Climatic and tectonic control on the Cenozoic evolution of the West African margin. *Marine Geology*, *178*(1–4), 63–80. [https://doi.org/10.1016/S0025-3227\(01\)00175-X](https://doi.org/10.1016/S0025-3227(01)00175-X)
- López-Mir, B., Muñoz, J. A., & García-Senz, J. (2016). 3D geometric reconstruction of Upper Cretaceous passive diapirs and salt withdrawal basins in the Cotiella Basin (southern Pyrenees). *Journal of the Geological Society*, *173*(4), 616–627. <https://doi.org/10.1144/jgs2016-002>
- Marsh, N., Imber, J., Holdsworth, R. E., Brockbank, P., & Ringrose, P. (2010). The structural evolution of the Halten Terrace, offshore Mid-Norway: Extensional fault growth and strain localisation in a multi-layer brittle–ductile system. *Basin Research*, *22*(2), 195–214. <https://doi.org/10.1111/j.1365-2117.2009.00404.x>
- Marton, G., Tari, G. C., & Lehmann, C. T. (2000). Evolution of the Angolan Passive Margin, West Africa, With Emphasis on Post-Salt Structural Styles. *Geophysical Monograph-American Geophysical Union*, *115*, 129–149.
- McBride, B. C., Rowan, M. G., & Weimer, P. (1998). The evolution of allochthonous salt systems, northern Green Canyon and Ewing Bank (offshore Louisiana), northern Gulf of Mexico. *AAPG Bulletin*, *82*(5), 1013–1036.
- Nürnberg, D., & Müller, R. D. (1991). The tectonic evolution of the South Atlantic from Late Jurassic to present. *Tectonophysics*, *191*(1), 27–53. [https://doi.org/10.1016/0040-1951\(91\)90231-G](https://doi.org/10.1016/0040-1951(91)90231-G)
- Oluboyo, A. P., Gawthorpe, R. L., Bakke, K., & Hadler-Jacobsen, F. (2014). Salt tectonic controls on deep-water turbidite depositional systems: Miocene, southwestern Lower Congo Basin, offshore Angola. *Basin Research*, *26*(4), 597–620. <https://doi.org/10.1111/bre.12051>
- Peel, F. J. (2014a). How do salt withdrawal minibasins form? Insights from forward modelling, and implications for hydrocarbon migration. *Tectonophysics*, *630*, 222–235. <https://doi.org/10.1016/j.tecto.2014.05.027>
- Peel, F. J. (2014b). The engines of gravity-driven movement on passive margins: Quantifying the relative contribution of spreading vs.

- gravity sliding mechanisms. *Tectonophysics*, 633, 126–142. <https://doi.org/10.1016/j.tecto.2014.06.023>
- Pichel, L. M., Peel, F., Jackson, C. A. L., & Huuse, M. (2018). Geometry and kinematics of salt-detached ramp syncline basins. *Journal of Structural Geology*, 115, 208–230. <https://doi.org/10.1016/j.jsg.2018.07.016>
- Prather, B. E., Booth, J. R., Steffens, G. S., & Craig, P. A. (1998). Classification, lithologic calibration, and stratigraphic succession of seismic facies of intraslope basins, deep-water Gulf of Mexico. *AAPG Bulletin*, 82(5), 701–728.
- Quirk, D. G., Schødt, N., Lassen, B., Ings, S. J., Hsu, D., Hirsch, K. K., & Von Nicolai, C. (2012). Salt tectonics on passive margins: Examples from Santos, Campos and Kwanza basins. *Geological Society, London, Special Publications*, 363(1), 207–244. <https://doi.org/10.1144/SP363.10>
- Roberts, M. J., Metzgar, C. R., Liu, J., & Lim, S. J. (2004). Regional assessment of salt weld timing, Campos Basin, Brazil. In P. J. Post, D. L. Olson, K. T. Lyons, S. L. Palmes, P. F. Harrison, & N. C. Rosen (Eds.), *Salt-Sediment Interactions and Hydrocarbon Prospectivity: Concepts, Applications, and Case Studies for the 21st Century* (pp. 371–389). Houston: Society of Economic Paleontologist and Mineralogists, Gulf Coast Section.
- Rowan, M. G. (1993). A systematic technique for the sequential restoration of salt structures. *Tectonophysics*, 228(3–4), 331–348. [https://doi.org/10.1016/0040-1951\(93\)90347-M](https://doi.org/10.1016/0040-1951(93)90347-M)
- Rowan, M. G. (2004). *Do Salt Welds Seal?* Paper presented at the Salt Sediment Interactions and Hydrocarbon Prospectivity Concepts, Applications and Case Studies for the, 21st Century. ed.
- Rowan, M. G., Lawton, T. F., & Giles, K. A. (2012). Anatomy of an exposed vertical salt weld and flanking strata, La Popa Basin, Mexico. *Geological Society, London, Special Publications*, 363(1), 33–57. <https://doi.org/10.1144/SP363.3>
- Rowan, M. G., Peel, F. J., & Vendeville, B. C. (2004). Gravity-driven fold belts on passive margins. In K. R. McClay (Ed.), *AAPG Memoir* (Vol. 82, pp. 157–182). Tulsa, OK: The American Association of Petroleum Geologists (AAPG).
- Rowan, M. G., & Weimer, P. (1998). Salt-sediment interaction, northern Green Canyon and Ewing bank (offshore Louisiana), northern Gulf of Mexico. *AAPG Bulletin*, 82(5), 1055–1082.
- Stewart, S. A. (2007). Salt tectonics in the North Sea Basin: A structural style template for seismic interpreters. In A. C. Ries, R. W. H. Butler, & R. H. Graham (Eds.), *Geological Society, London, Special Publications* (Vol. 272, pp. 361–396). <https://doi.org/10.1144/GSL.SP.2007.272.01.19>
- Stewart, S. A., & Clark, J. A. (1999). Impact of salt on the structure of the Central North Sea hydrocarbon fairways. Paper presented at the Geological Society, London, Petroleum Geology Conference series
- Trudgill, B. D. (2011). Evolution of salt structures in the northern Paradox Basin: Controls on evaporite deposition, salt wall growth and supra-salt stratigraphic architecture. *Basin Research*, 23(2), 208–238. <https://doi.org/10.1111/j.1365-2117.2010.00478.x>
- Valle, P. J., Gjelberg, J. G., & Helland-Hansen, W. (2001). Tectonostratigraphic development in the eastern Lower Congo Basin, offshore Angola, west Africa. *Marine and Petroleum Geology*, 18(8), 909–927. [https://doi.org/10.1016/S0264-8172\(01\)00036-8](https://doi.org/10.1016/S0264-8172(01)00036-8)
- Vendeville, B. C. (2005). Salt tectonics driven by sediment progradation: Part I—Mechanics and kinematics. *AAPG Bulletin*, 89(8), 1071–1079. <https://doi.org/10.1306/03310503063>
- Vendeville, B. C., & Jackson, M. P. A. (1992). The fall of diapirs during thin-skinned extension. *Marine and Petroleum Geology*, 9(4), 354–371. [https://doi.org/10.1016/0264-8172\(92\)90048-J](https://doi.org/10.1016/0264-8172(92)90048-J)
- Wagner, B. H. (2010). *An analysis of salt welding*. (PhD), University of Texas at Austin.
- Wagner, B. H., & Jackson, M. P. A. (2011). Viscous flow during salt welding. *Tectonophysics*, 510(3), 309–326. <https://doi.org/10.1016/j.tecto.2011.07.012>
- Warsitzka, M., Kley, J., & Kukowski, N. (2013). Salt diapirism driven by differential loading — Some insights from analogue modelling. *Tectonophysics*, 591, 83–97. <https://doi.org/10.1016/j.tecto.2011.11.018>
- Weimer, P., Bouroullec, R., van den Berg, A. A., Lapinski, T. G., Roesink, J. G., & Adson, J. (2017). Structural setting and evolution of the Mensa and Thunder Horse intraslope basins, northern deep-water Gulf of Mexico: A case study. *AAPG Bulletin*, 101(7), 1145–1172. <https://doi.org/10.1306/09011609112>
- Worrall, D. M., & Snelson, S. (1989). Evolution of the northern Gulf of Mexico, with emphasis on Cenozoic growth faulting and the role of salt. In A. W. Bally, & A. R. Palmer (Eds.), *The Geology of North America-An Overview* (pp. 97–137). Boulder, CO: Geological Society of America, Inc.

**How to cite this article:** Ge Z, Gawthorpe RL, Rotevatn A, Zijerveld L, A.-L. Jackson C, Oluboyo A. Minibasin depocentre migration during diachronous salt welding, offshore Angola. *Basin Res.* 2019;00: 1–19. <https://doi.org/10.1111/bre.12404>